Magneto-Chiral Dichroism in a One-Dimensional Assembly of Helical Dysprosium(III) Single-Molecule Magnets

Maria Sara Raju, Kais Dhbaibi, Maxime Grasser, Vincent Dorcet, Ivan Breslavetz, Kevin Paillot, Nicolas Vanthuyne, Olivier Cador, Rikken G.L.J.A., Boris Le Guennic, et al.

▶ **To cite this version:**

Maria Sara Raju, Kais Dhbaibi, Maxime Grasser, Vincent Dorcet, Ivan Breslavetz, et al.. Magneto-Chiral Dichroism in a One-Dimensional Assembly of Helical Dysprosium(III) Single-Molecule Magnets. Inorganic Chemistry, 2023, 62 (43), pp.17583-17587. 10.1021/acs.inorgchem.3c03204 . hal-04262652

HAL Id: hal-04262652
https://hal.science/hal-04262652

Submitted on 17 Nov 2023

HAL is a multi-disciplinary open access archive for the deposit and dissemination of scientific research documents, whether they are published or not. The documents may come from teaching and research institutions in France or abroad, or from public or private research centers.

L'archive ouverte pluridisciplinaire **HAL**, est destinée au dépôt et à la diffusion de documents scientifiques de niveau recherche, publiés ou non, émanant des établissements d'enseignement et de recherche français ou étrangers, des laboratoires publics ou privés.

Magneto-Chiral Dichroism in a One-dimensional Assembly of Helical Dysprosium(III) Single-Molecule Magnets

Maria Sara Raju,[†] Kais Dhbaibi,[‡] Maxime Grasser,[‡] Vincent Dorcet,[‡] Ivan Breslavetz,[†] Kévin Paillot,[†] Nicolas Vanthuyne,[‖] Olivier Cador,[‡] Geert L. J. A. Rikken,[†] Boris Le Guennic,[‡] Jeanne Crassous,[‡] Fabrice Pointillart,[‡] Cyrille Train[†] and Matteo Atzori*[†]

† Laboratoire National des Champs Magnétiques Intenses (LNCMI), Univ. Grenoble Alpes, INSA Toulouse, Univ. Toulouse Paul Sabatier, EMFL, CNRS, Grenoble, France

‡ Univ Rennes, CNRS, ISCR (Institut des Sciences Chimiques de Rennes) – UMR 6226, F-35000 Rennes, France

|| Aix Marseille University, CNRS, Centrale Marseille, iSm2 Marseille, France

Supporting Information Placeholder

ABSTRACT: Here we report Magneto-Chiral Dichroism (MChD) detected through Visible and Near Infrared light absorption of a chiral Dy^{III} coordination polymer. The two enantiomers of $[Dy^{III}(H6(py)_2)(hfac)_3]_n$ ($H6(py)_2$ = 2,15-bis-(4-pyridyl)ethynyl-carbo[6]helicene; $hfac^-$ = 1,1,1,5,5,5-hexafluoroacetylacetonate), where the chirality is provided by a functionalized helicene ligand, were structurally, spectroscopically and magnetically investigated. Magnetic measurements reveal a slow relaxation of the magnetization, with differences between enantiopure and racemic systems rationalized on the basis of theoretical calculations. When the enantiopure complexes are irradiated with unpolarized light in a magnetic field they exhibit multiple MChD signals associated with the *f-f* electronic transitions of Dy^{III}, thus providing coexistence of MChD-active absorptions and Single-Molecule Magnet (SMM) behavior. These findings clearly show the potential that rationally designed chiral SMMs have in enabling the optical readout of magnetic memory through MChD.

Magneto-Chiral Dichroism (MChD) is a magneto-chiral effect that features a differential absorption or emission of unpolarized light that chiral systems exhibit when a magnetic field is applied collinearly to a light propagation wavevector.[1–3] It represents a fascinating manifestation of light-chiral matter interaction because neither unpolarized light nor magnetic fields are chiral *per se*. However, when associated, these physical entities provide a true chiral influence on chiral systems.[4,5]

Analogously to natural circular dichroism, MChD provides spectral responses equal in magnitude but opposite in sign for two enantiomers,[1–3] and analogously to magnetic circular dichroism, the signals intensity is intrinsically correlated to the system's magnetization.[6] For this reason, a potential technological application is the optical readout of magnetic data.[7–9] This consists in discriminating two orientations of the magnetization of a magnetic material by measuring a differential absorption or emission of unpolarized light, with a low-energy and non-damaging light source (Vis-NIR), without the need of circular polarization.

After the first observation of MChD through visible light emission,[1] MChD has been proven to be universal, with reports showing its observation in the entire electromagnetic spectrum (from hard X-rays to microwaves).[10–20]

Nowadays, the field is rapidly expanding among the chemistry community for the general interest that chiral systems have raised in several fields, such as chiroptical switching and sensing,[21] circularly polarized light emission,[22,23] chiral induced spin selectivity,[24,25] to cite a few.

For molecular systems, MChD investigations in the UV-Vis-NIR range are particularly interesting because different electronic transitions can be probed, spanning from that of purely organic systems,[26] transition metal-based,[18–20,27] to lanthanide-based systems.[10,28,29]

Because of the strong spin-orbit coupling and the magnetic-dipole character of some *f-f* transitions, recent studies have been focused on lanthanide complexes[10,28,29] or heterometallic 3*d*-4*f* chiral clusters.[30] Among them, two chiral Yb^{III} complexes have been investigated, a monomeric[29] and a polymeric[28] system, both containing helicene-based chiral ligands. The combination of the intrinsic chirality of the helicenic moiety with the properties of the lanthanide was found responsible for strong magneto-chiral responses (g_{MChD} 0.12-0.19 T^{-1}), and measurable MChD signals up to room temperature.[28]

To exploit such results in view of our ultimate goal of demonstrating optical readout of magnetic data through MChD, passing from Yb^{III} to Dy^{III}-based systems is a logic choice because the latter have shown the best SMM properties ever reported.[31]

Accordingly, we have targeted the Dy^{III} analogue of the Yb^{III} compound that has shown the best MChD properties. We have prepared enantiopure Dy^{III} complexes formulated as $[Dy^{III}(H6(py)_2)(hfac)_3]_n$, **1-*(P)*** and **1-*(M)***, and their racemic version **1-*(rac)***. Complexes **1-*(P)*** and **1-*(M)*** are obtained by reaction of enantiopure ***(P)***- and ***(M)***-$H6(py)_2$ with $[Dy^{III}(hfac)_3(H_2O)_2]$ in toluene (see SI). Layering *n*-hexane into the toluene solution gave single crystals suitable for X-ray diffraction analysis and MChD measurements. The optical activity was checked by natural circular dichroism spectroscopy in solution and solid-state (Figures S1-S4). **1-*(P)*** and **1-*(M)*** crystallize in the orthorhombic $P2_12_12_1$ space group (Table S1) and are isostructural to the Yb^{III} analogues.[28] They feature one crystallographically independent molecule where

the Dy^{III} is octacoordinated in a slightly distorted D_{2d} symmetry. The pyridine-functionalized helicene ligand coordinates the Dy^{III} in opposite axial positions, while the three *hfac* ligands are disposed on the plane (Figures 1 and S5-S6). The crystal structure shows a polymeric arrangement between different units where a π–π stacking between helicene aromatic rings of adjacent molecules develops along the *a* axis (Figure S7). Overall, the helicene-based ligand drives the chiral features of the crystal structure and asymmetrically distorts the coordination geometry of the lanthanide ion, that provides spin-orbit coupling and magnetic anisotropy.

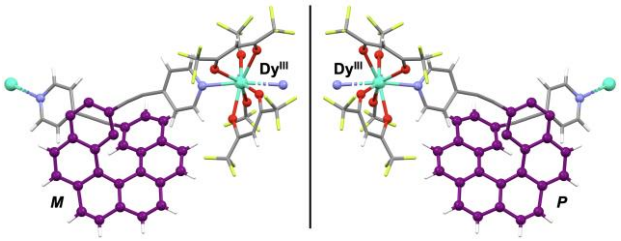

Figure 1. Molecular structures of **1-*(M)*** and **1-*(P)*** with helical helicity of the ligand and lanthanide center highlighted.

In contrast, **1-*(rac)*** crystallizes in the monoclinic *C*2 space group with two independent Dy^{III} centers and two helicene ligands with opposite chirality (Figure S8). Racemic mixture which crystallizes in chiral space group might be attributed of the kryptoracemate. The coordination geometries around the two Dy^{III} ions are very similar (slightly distorted achiral D_{4d} symmetry). Within the 1D polymeric backbone the helicene ligands display an alternation of *P* and *M* chirality. Moreover, the crystal structure also shows a supramolecular arrangement along the *b* axis for which all the helicenic ligands possess the same chirality (Figure S9).

At room temperature, $\chi_M T$ (molar magnetic susceptibility times the temperature) values for **1-*(P)*** and **1-*(rac)*** are 13.98 and 14.02 cm^3 K mol^{-1}, respectively, and are consistent with the expected value (14.17 cm^3 K mol^{-1}) for an isolated $^6H_{15/2}$ multiplet ground state (Figure S10). At T = 2.0 K, the magnetization saturates at values close to 5 μ_B mol^{-1} for both compounds, in agreement with the stabilization of M_J = ±15/2 Kramers doublet (Figure S10). The dynamic magnetic properties were also investigated by alternating current susceptibility measurements (AC). At 2 K and zero field, both materials show out-of-phase components (χ_M'') (Figures S11-S12) that indicate a slowing down of the magnetization relaxation. The χ_M'' maxima shift to lower frequencies when a magnetic field is applied, with the slowest relaxation occurring at 1 kOe for **1-*(P)*** and 1.8 kOe for **1-*(rac)***. For **1-*(P)***, at the optimum field of 1 kOe the AC data can be analyzed in the frame of the extended Debye model (Figures S12-S13, Table S2). α values are close to 0.2 whatever the temperature, with a non-relaxing fraction (χ_S/χ_T) close to 15%, which means that almost all magnetic moments are concerned by the slow relaxation. The T dependence of the relaxation time (Figure S14) can be reproduced with a Raman process ($\tau^{-1} = CT^n$) with C = 3.3(2) s^{-1} K^{-n} and n = 4.30(3) as best-fit parameters.

To support the magnetic data, wavefunction-based multiconfigurational CAS(9,7)SCF calculations have been carried out on **1-(*P*)** and **1-(*rac*)**. For the latter, the two Dy^{III} centers have been modeled separately (**a** and **b**) (see SI). Theoretical calculations are in good agreement with the observed magnetic properties, showing that the Kramers doublet ground state is dominated by M_J = ±15/2 (Table S3). At room temperature, $\chi_M T$ is calculated higher for **1-(*rac*)** (averaged over **a** and **b**) than for **1-(*P*)** (13.95 and 13.35 cm^3 K mol^{-1}, respectively). The comparisons with the experimental data are reported in Figure S10. Magnetic anisotropic ***g*** tensors and easy axes of the ground states were also calculated (Figure S15). Interestingly, the two Dy^{III} sites along the polymeric chain of **1-(*rac*)** do not exhibit the same easy axis orientation and have a slightly different composition of the ground state wavefunction which could partially explain the broadening and the distortion of the AC out-of-phase component. This is also visible in the computed magnetization blocking barriers (Figure S16).

Single crystals of **1-*(P)*** and **1-*(M)*** (ca. 0.8×0.8×0.15 mm) were used to record absorption spectra in transmission mode with Vis-NIR unpolarized light propagating along the *c* axis. The wide-range (440-1550 nm) absorption spectrum at 4.0 K is reported in Figure S17 while the thermal variation up to 150 K of the main absorption bands is reported in Figure 2.

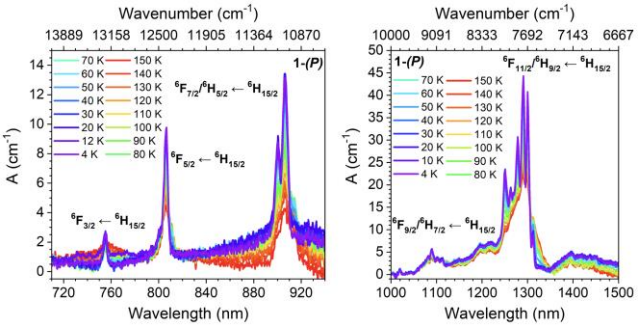

Figure 2. Thermal variation of the absorption coefficient for a single crystal of **1-*(P)*** (***k***||*c*) in the (left) 720-940 nm and (right) 1000-1500 nm ranges.

The investigated range shows multiple sharp absorption peaks associated with the *f-f* transitions between the $^6H_{15/2}$ Dy^{III} ground state and the energy levels of the ^6F and/or ^6H spectroscopic terms, as detailed in Table 1.[30,32–34]

Table 1. Assignment of the Dy^{III} absorption peaks

λ (nm)	***f-f* transition assignment**
755	$^6F_{3/2}$←$^6H_{15/2}$
806	$^6F_{5/2}$←$^6H_{15/2}$
906	$^6F_{7/2}$/$^6H_{5/2}$←$^6H_{15/2}$
1060-1120	$^6F_{9/2}$/$^6H_{7/2}$←$^6H_{15/2}$
1240-1320	$^6F_{11/2}$/$^6H_{9/2}$←$^6H_{15/2}$

The $^4F_{9/2}$←$^6H_{15/2}$ and $^4I_{15/2}$←$^6H_{15/2}$ transitions, typically observed between 400 and 500 nm, are not detected, being superimposed with the much more intense ligand absorption.

MChD measurements were performed at T = 4.0 K with an alternating magnetic field ***B*** applied along ***k*** in the 0.0–2.0 T range. Figure 3 shows the magnetic field dependence of the MChD spectra for **1-*(P)***.

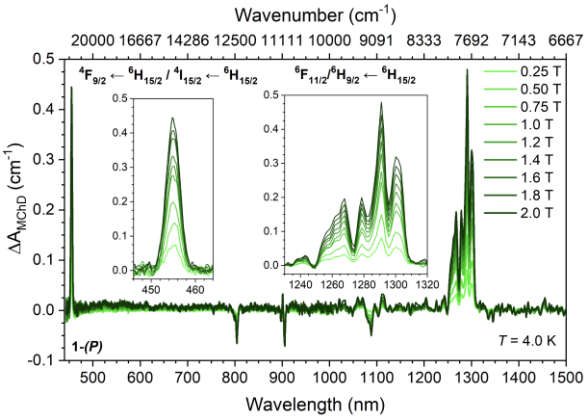

Figure 3. Magnetic field dependence of ΔA_{MChD} for **1-*(P)*** at T = 4.0 K. Insets show the details of the most intense MChD signals.

MChD signals are observed for each electronic transition detected in absorption. Interestingly, even if the $^4F_{9/2}\leftarrow{}^6H_{15/2}$ and $^4I_{15/2}\leftarrow{}^6H_{15/2}$ absorptions are not observed due to the superposition with the ligand absorption, a strong and sharp MChD signal is observed at ca. 455 nm (Figure 3). The other intense MChD response is related to the fine-structured absorption of the $^6F_{11/2}/^6H_{9/2}\leftarrow{}^6H_{15/2}$ transition. For this multiplet, the absorption coefficients at zero field are available (Figure 2), therefore, the g_{MChD} asymmetry factor can be determined. For the two sharp peaks at λ = 1291 and 1300 nm, at $\boldsymbol{B}$ = 1.0 T, g_{MChD} assumes values of ca. 1.2% and 0.9%, respectively. These relatively low values, despite a strong ΔA_{MChD} response, are due to the strong absorption coefficients of the originating transition. Indeed, the high value of the absorption coefficient agrees with its hypersensitive character, that obeys to selection rules similar to that of quadrupolar transitions.[35,36]

It is instructive to calculate the g_{MChD} asymmetry factor for those transitions that provide MChD signals with lower absolute values, but associated with a low absorption coefficient. This is the case of the $^6F_{5/2} \leftarrow {}^6H_{15/2}$, and $^6F_{7/2}/^6H_{5/2}\leftarrow{}^6H_{15/2}$ transitions. Under the same field, they provide g_{MChD} of 0.8% and 0.7%, thus of the same order of magnitude of the previously analyzed transitions.

Overall, the estimated g_{MChD} values are one order of magnitude lower than that observed for the Yb^{III} analogue. These results can be rationalized considering the nature of the investigated electronic transitions. None of them is magnetic dipole allowed (ΔJ = 0, ±1), contrarily to the Yb^{III} $^2F_{5/2}\leftarrow{}^2F_{7/2}$ transition, and because electric-dipole transitions are parity forbidden (Laporte selection rule), all of them are considered induced electric dipole transitions (Judd-Ofelt theory).[35,36] Therefore, since the chiral environment around the lanthanide ion is the same, being the Dy^{III} and Yb^{III} systems isostructural, as well as the probed crystal orientation, the relatively low values of g_{MChD} for Dy^{III} can be associated with the lack of magnetic dipole allowed character of the investigated transitions.

MChD measurements were also performed as a function of the temperature. Figure 4 shows the thermal variation of the MChD spectra for both enantiomers.

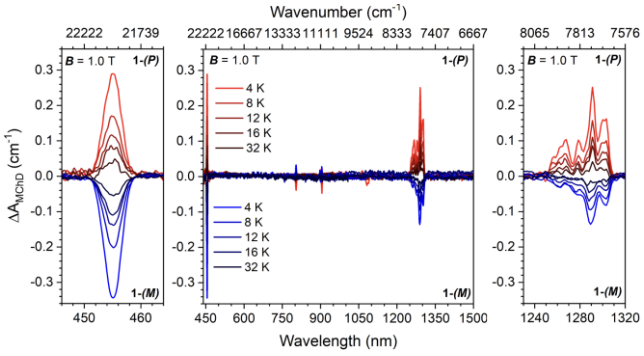

Figure 4. Temperature dependence of ΔA_{MChD} at $\boldsymbol{B}$ = 1.0 T for **1-*(M)*** and **1-*(P)***. Lateral panels show the details of the most intense transitions. The difference in the relative intensity among high and low energy signals is ascribed to a slightly different orientation of the probed crystals.

MChD signals with similar intensities and opposite signs for the two enantiomers are observed (Figure SX). As the temperature increases, the intensity of the MChD signals decreases, without a significant change in the signals shape. For higher temperatures the signal intensities were below the detection limits of our experimental setup.

These results can be rationalized by analyzing the signal at 455 nm, which is intense and well separated from other transitions. Having an absorption-like shape, it evidences that a T dependent Faraday C term mechanism, associated to a change in the population of the ground state, is at the origin of the MChD.[29] Figure 5 shows the temperature and the magnetic field dependence of ΔA_{MChD} at two wavelengths for both enantiomers compared with magnetization data recorded in the same conditions on a microcrystalline sample of **1-*(P)***.

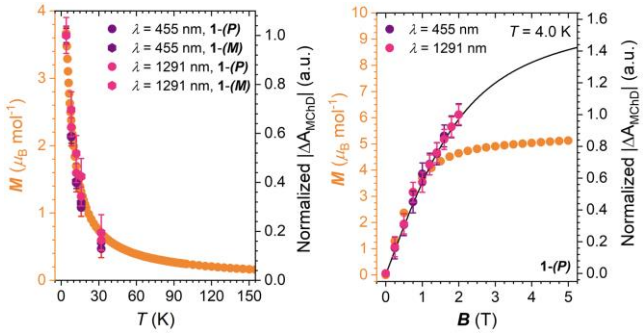

Figure 5. Temperature (a) and magnetic field (b) dependence of ΔA_{MChD} (λ = 455, 1291 nm) for **1-*(M)*** and **1-*(P)*** compared to magnetization data. The black line is the simulated magnetization curve based on the Brillouin function assuming $\mathbf{g}_J$ = 4/3 and J = 15/2.

ΔA_{MChD} accurately follows the temperature dependence of the sample magnetization independently from the nature of the investigated transition, confirming that a C term underlying mechanism dominates between 4 and 32 K, as expected for a system with uniaxial magnetic anisotropy. When the ΔA_{MChD} values at T = 4.0 K are compared to the $\boldsymbol{B}$ dependence of the magnetization, it can be observed that the intensity increases linearly, and at 2.0 T, it does not reach saturation, contrarily to the case of the microcrystalline powder. This can be explained by the fact that MChD measurements have been done on oriented single crystals. For Dy^{III} systems featuring non-interacting magnetic ions, as for **1**, the expected M_S value is ca. 5 μ_B mol^{-1} if magnetic measurements are performed on a randomly oriented powder, and 10 μ_B mol^{-1} if they are performed along the magnetization easy axis.[37] Although our current setup is limited to $\boldsymbol{B}$ = 2 T, the experimental data clearly show that the ΔA_{MChD} variation follows the expected behavior for an oriented single-crystal (black line in Figure 5). Indeed, theoretical calculations estimate a magnetization easy axis oriented, although not exactly parallel, along the probed c axis (Figure S15), in agreement with the experimental findings.

In conclusion, we have investigated a chiral Dy^{III} 1D-polymer that exhibits coexistence of SMM properties and MChD in the same temperature range. In the Vis-NIR region, multiple MChD signals have been observed. Although with modest g_{MChD} values when compared to the Yb^{III} analogue, all probed transitions are MChD-active, and their intensity follows the T and $\boldsymbol{B}$ dependence of the system magnetization at multiple wavelengths. These findings indicate that the optical sensing of the magnetic state of SMMs with unpolarized light through MChD is viable on rationally designed chiral SMMs.

ASSOCIATED CONTENT

Supporting Information

Additional figures, tables and experimental section as mentioned in the text.

AUTHOR INFORMATION

Corresponding Authors

matteo.atzori@lncmi.cnrs.fr

Notes

The authors declare no competing financial interests.

ACKNOWLEDGMENT

The French National Research Agency (ANR) and the European Research Council (ERC) are acknowledged for financial support through MONAFER (ANR-18-CE09-0032), SMMCPL (ANR-19-CE29-0012-02) and MaChiNaCo (ANR-19-CE09-0018) projects and the European Union's Horizon 2020 research and innovation program (ERC-CoG MULTIPROSMM, grant agreement N°725184). This project has received financial support from the CNRS through the MITI interdisciplinary programs through its exploratory research program. The French GENCI/IDRIS-CINES centers for high-performance computing resources are also acknowledged.

REFERENCES

(1) Rikken, G. L. J. A.; Raupach, E. Observation of Magneto-Chiral Dichroism. *Nature* **1997**, *390*, 493–494.

(2) Atzori, M.; Rikken, G. L. J. A.; Train, C. Magneto-Chiral Dichroism: A Playground for Molecular Chemists. *Chem. Eur. J.* **2020**, *26*, 9784–9791.

(3) Atzori, M.; Train, C.; Hillard, E. A.; Avarvari, N.; Rikken, G. L. J. A. Magneto-chiral Anisotropy: From Fundamentals to Perspectives. *Chirality* **2021**, *33*, 844–857.

(4) Barron, L. D. Symmetry and Molecular Chirality. *Chem. Soc. Rev.* **1986**, *15*, 189.

(5) Barron, L. D. True and False Chirality and Parity Violation. *Chem. Phys. Lett.* **1986**, *123*, 423–427.

(6) Stephens, P. J. Theory of Magnetic Circular Dichroism. *J. Chem. Phys.* **1970**, *52*, 3489.

(7) Galán-Mascarós, J. R. Bring to Light. *Nat. Phys.* **2015**, *11*, 7–8.

(8) Barron, L. D. Chirality, Magnetism and Light. *Nature* **2000**, *405*, 895–896.

(9) Barron, L. D. Chirality and Magnetism Shake Hands. *Nat. Mater.* **2008**, *7* (9), 691–692.

(10) Taniguchi, K.; Kishiue, S.; Kimura, S.; Miyasaka, H. Local-Site Dependency of Magneto-Chiral Dichroism in Enantiopure One-Dimensional Copper(II)–Chromium(III) Coordination Polymers. *J. Physical. Soc. Japan.* **2019**, *88*, 93708.

(11) Taniguchi, K.; Nishio, M.; Kishiue, S.; Huang, P.-J.; Kimura, S.; Miyasaka, H. Strong Magnetochiral Dichroism for Visible Light Emission in a Rationally Designed Paramagnetic Enantiopure Molecule. *Phys. Rev. Mater.* **2019**, *3*, 45202.

(12) Tomita, S.; Sawada, K.; Kurosawa, H.; Ueda, T. Magnetochiral Metamolecules for Microwaves. In *Springer Series in Materials Science*; 2019.

(13) Okamura, Y.; Kagawa, F.; Seki, S.; Kubota, M.; Kawasaki, M.; Tokura, Y. Microwave Magnetochiral Dichroism in the Chiral-Lattice Magnet Cu2OSeO3. *Phys. Rev. Lett.* **2015**, *114*, 197202.

(14) Tomita, S.; Sawada, K.; Porokhnyuk, A.; Ueda, T. Direct Observation of Magnetochiral Effects through a Single Metamolecule in Microwave Regions. *Phys. Rev. Lett*. **2014**, *113*, 235501.

(15) Sessoli, R.; Boulon, M.-E.; Caneschi, A.; Mannini, M.; Poggini, L.; Wilhelm, F.; Rogalev, A. Strong Magneto-Chiral Dichroism in a Paramagnetic Molecular Helix Observed by Hard X-Rays. *Nat. Phys.* **2015**, *11*, 69–74.

(16) Mitcov, D.; Platunov, M.; Buch, C. D.; Reinholdt, A.; Døssing, A. R.; Wilhelm, F.; Rogalev, A.; Piligkos, S. Hard X-Ray Magnetochiral Dichroism in a Paramagnetic Molecular 4f Complex. *Chem. Sci.* **2020**, *11*, 8306–8311.

(17) Train, C.; Gheorghe, R.; Krstic, V.; Chamoreau, L.-M.; Ovanesyan, N. S.; Rikken, G. L. J. A.; Gruselle, M.; Verdaguer, M. Strong Magneto-Chiral Dichroism in Enantiopure Chiral Ferromagnets. *Nat. Mater.* **2008**, *7*, 729–734.

(18) Atzori, M.; Ludowieg, H.; Cortijo, M.; Breslavetz, I.; Paillot, K.; Rosa, P.; Train, C.; Autschbach, J.; Hillard, E. A.; Rikken, G. L. J. A. Validation of Microscopic Magneto-Chiral Dichroism Theory. *Sci. Adv.* **2021**, *7*, eabg2859–eabg2859.

(19) Atzori, M.; Breslavetz, I.; Paillot, K.; Inoue, K.; Rikken, G. L. J. A.; Train, C. A Chiral Prussian Blue Analogue Pushes Magneto-Chiral Dichroism Limits. *J. Am. Chem. Soc.* **2019**, *141*, 20022–20025.

(20) Atzori, M.; Santanni, F.; Breslavetz, I.; Paillot, K.; Caneschi, A.; Rikken, G. L. J. A.; Sessoli, R.; Train, C. Magnetic Anisotropy Drives Magnetochiral Dichroism in a Chiral Molecular Helix Probed with Visible Light. *J. Am. Chem. Soc.* **2020**, *142*, 13908–13916.

(21) Staszak, K.; Wieszczycka, K.; Marturano, V.; Tylkowski, B. Lanthanides Complexes – Chiral Sensing of Biomolecules. *Coord. Chem. Rev.* **2019**, *397*, 76–90.

(22) Zinna, F.; Di Bari, L. Lanthanide Circularly Polarized Luminescence: Bases and Applications. *Chirality* **2015**, *27*, 1–13.

(23) Willis, O. G.; Zinna, F.; Di Bari, L. NIR-Circularly Polarized Luminescence from Chiral Complexes of Lanthanides and D-Metals. *Angew. Chem. Int. Ed.* **2023**, *135*, e202302358.

(24) Gohler, B.; Hamelbeck, V.; Markus, T. Z.; Kettner, M.; Hanne, G. F.; Vager, Z.; Naaman, R.; Zacharias, H. Spin Selectivity in Electron Transmission Through Self-Assembled Monolayers of Double-Stranded DNA. *Science (1979)* **2011**, *331*, 894–897.

(25) Naaman, R.; Paltiel, Y.; Waldeck, D. H. Chiral Molecules and the Electron Spin. *Nat. Rev. Chem.* **2019**, *3*, 250–260.

(26) Kitagawa, Y.; Segawa, H.; Ishii, K. Magneto-Chiral Dichroism of Organic Compounds. *Angew. Chem. Int. Ed.* **2011**, *50*, 9133–9136.

(27) Atzori, M.; Breslavetz, I.; Paillot, K.; Rikken, G. L. J. A.; Train, C. Role of Structural Dimensionality in the Magneto-Chiral Dichroism of Chiral Molecular Ferrimagnets. *J. Mater. Chem. C* **2022**, *10*, 13939–13945.

(28) Dhbaibi, K.; Grasser, M.; Douib, H.; Dorcet, V.; Cador, O.; Vanthuyne, N.; Riobé, F.; Maury, O.; Guy, S.; Bensalah-Ledoux, A.; Baguenard, B.; Rikken, G. L. J. A.; Train, C.; Le Guennic, B.; Atzori, M.; Pointillart, F.; Crassous, J. Multifunctional Helicene-Based Ytterbium Coordination Polymer Displaying Circularly Polarized Luminescence, Slow Magnetic Relaxation and Room Temperature Magneto-Chiral Dichroism. *Angew. Chem. Int. Ed.* **2023**, *135*, e.202215558.

(29) Atzori, M.; Dhbaibi, K.; Douib, H.; Grasser, M.; Dorcet, V.; Breslavetz, I.; Paillot, K.; Cador, O.; Rikken, G. L. J. A.; Le Guennic, B.; Crassous, J.; Pointillart, F.; Train, C. Helicene-Based Ligands Enable Strong Magneto-Chiral Dichroism in a Chiral Ytterbium Complex. *J. Am. Chem. Soc.* **2021**, *143*, 2671–2675.

(30) Wang, X.; Wang, S.-Q.; Chen, J.-N.; Jia, J.-H.; Wang, C.; Paillot, K.; Breslavetz, I.; Long, L.-S.; Zheng, L.; Rikken, G. L. J. A.; Train, C.; Kong, X.-J.; Atzori, M. Magnetic 3d–4f Chiral Clusters Showing Multimetal Site Magneto-Chiral Dichroism. *J. Am. Chem. Soc.* **2022**, *144*, 8837–8847.

(31) Guo, F.-S.; Day, B. M.; Chen, Y.-C.; Tong, M.-L.; Mansikkamäki, A.; Layfield, R. A. Magnetic Hysteresis up to 80 Kelvin in a Dysprosium Metallocene Single-Molecule Magnet. *Science* **2018**, *362*, 1400–1403.

(32) Perfetti, M.; Gysler, M.; Rechkemmer-Patalen, Y.; Zhang, P.; Taştan, H.; Fischer, F.; Netz, J.; Frey, W.; Zimmermann, L. W.; Schleid, T.; Hakl, M.; Orlita, M.; Ungur, L.; Chibotaru, L.; Brock-Nannestad, T.; Piligkos, S.; van Slageren, J. Determination of the Electronic Structure of a Dinuclear Dysprosium Single Molecule Magnet without Symmetry Idealization. *Chem. Sci.* **2019**, *10*, 2101–2110.

(33) Comba, P.; Daumann, L. J.; Klingeler, R.; Koo, C.; Riley, M. J.; Roberts, A. E.; Wadepohl, H.; Werner, J. Correlation of Structural and Magnetic Properties in a Set of Mononuclear Lanthanide Complexes. *Chem. Eur. J.* **2018**, *24*, 5319–5330.

(34) Comba, P.; Großhauser, M.; Klingeler, R.; Koo, C.; Lan, Y.; Müller, D.; Park, J.; Powell, A.; Riley, M. J.; Wadepohl, H. Magnetic Interactions in a Series of Homodinuclear Lanthanide Complexes. *Inorg. Chem.* **2015**, *54*, 11247–11258.

(35) Richardson, F. S. Selection Rules for Lanthanide Optical Activity. *Inorg. Chem.* **1980**, *19*, 2806–2812.

(36) Bünzli, J.-C. G. On the Design of Highly Luminescent Lanthanide Complexes. *Coord. Chem. Rev.* **2015**, *293–294*, 19–47.

(37) Briganti, M.; Lucaccini, E.; Chelazzi, L.; Ciattini, S.; Sorace, L.; Sessoli, R.; Totti, F.; Perfetti, M. Magnetic Anisotropy Trends along a Full 4f-Series: The f^{n+7} Effect. *J. Am. Chem. Soc.* **2021**, *143*, 8108–8115.

TOC Graphic

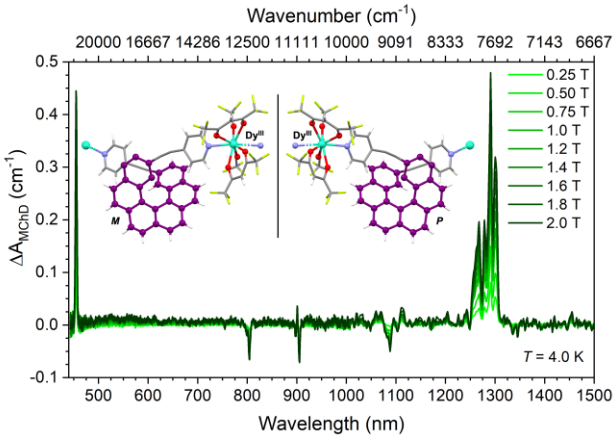

Here we report on a one-dimensional assembly of helical Dysprosium(III) Single-Molecule Magnets that exhibits coexistence of SMM properties and Magneto-Chiral Dichroism. Although with modest g_{MChD} values, all probed transitions are MChD-active, and their intensity follows the temperature and magnetic field dependence of the system magnetization at multiple wavelengths. These findings indicate that the optical sensing of the magnetic state of SMMs with unpolarized light through MChD is viable on rationally designed chiral SMMs.